Journal of Solid State Chemistry 184 (2011) 1120–1128

Contents lists available at ScienceDirect

Journal of Solid State Chemistry

journal homepage: www.elsevier.com/locate/jssc

X-rays structural analysis and thermal stability studies of the ternary compound α-AlFeSi

J. Roger *, F. Bosselet, J.C. Viala

Laboratoire des Multimatériaux et Interfaces, UMR CNRS no. 5615, Université Claude Bernard Lyon 1, F-69622 Villeurbanne Cedex, France

ARTICLE INFO

Article history:
Received 11 January 2011
Received in revised form
8 March 2011
Accepted 13 March 2011
Available online 21 March 2011

Keywords:
Aluminide
Ternary phase
Solid solution
Solid state reaction
Crystal structure
Thermal analysis

ABSTRACT

From literature data presently available, the decomposition temperature and the nature of the decomposition reaction of the ternary compound α-AlFeSi (also designated as α_H or τ_5) are not clearly identified. Moreover, some uncertainties remain concerning its crystal structure. The crystallographic structure and thermochemical behaviour of the ternary compound α-AlFeSi were meticulously studied. The crystal structure of α-AlFeSi was examined at room temperature from X-ray single crystal intensity data. It presents hexagonal symmetry, space group $P6_3/mmc$ with unit cell parameters (293 K) $a=12.345(2)$ Å and $c=26.210(3)$ Å ($V=3459$ Å^3). The average chemical formula obtained from refinement is $Al_{7.1}Fe_2Si$. From isothermal reaction-diffusion experiments and Differential Thermal Analysis, the title compound decomposes peritectically upon heating into θ-Fe_4Al_{13}(Si), γ-Al_3FeSi and a ternary Al-rich liquid. Under atmospheric pressure, the temperature of this reversible transformation has been determined to be 772 ± 12 °C.

1. Introduction

Production of sheets and castings based on aluminium alloys as well as development of aluminium/steel assemblies require a thorough knowledge of the phase diagrams of the relevant systems. Chemical instabilities and mechanical embrittlement owing to the interface reactions between aluminium alloys and iron are critical parameters that have to be carefully examined [1–4]. Considering that the major constituent of many aluminides is silicon, the Fe–Al–Si system has been the subject of many experimental investigations [5–8]. The results of those experimental studies were summarised in several publications [9–12]. Thermodynamic assessments of the whole system based on the CALPHAD method have also been proposed first by Liu and Chang [13] and more recently by Du et al. [14]. Malakhov et al. [15] developed predictive calculations based on the Scheil's formalism and the concept of driving forces to explain the formation of metastable compounds during supercooling. The main feature of this system is the occurrence of numerous ternary phases. Up to now, ten different phases labelled from τ_1 to τ_{11} ($\tau_1=\tau_9$) have been isolated and crystallised directly either from the liquid or through invariant or monovariant reactions [6–7,10,13]. All the phases exhibit homogeneity ranges more or less extended with an iron concentration practically constant [13,16]. It is worth noting that the silicon limit of the homogeneity range can vary with temperature [13]. Several studies have involved the reaction scheme in the aluminium rich corner of the system that is the more critical regarding the potential applications *i.e.* metal joining between iron and aluminium–silicon alloys [7,15,17]. Among those Al-rich phases, several structural and/or thermochemical data are not available or incomplete.

Our attention in the present work was focused on the compound α-AlFeSi (also designated as α_H or τ_5) with average chemical formula $Al_{7.1}Fe_2Si$. From literature, this phase is known to form very easily by crystallisation from ternary Al-rich melts, as shown in Fig. 1 [5,6,17,18]. This ternary compound is characterised by a hexagonal symmetry, space group $P6_3/mmc$ with unit cell $a=12.404(1)$ Å and $c=26.234(2)$ Å but the crystallographic structure is neither precisely depicted nor fully understood [18,19]. It also exhibits a homogeneity range that varies with temperature [16,17,20]. Literature reports enthalpies of formation $\Delta_f H^0$ at 25 °C of -34.3 ± 2 kJ mol^{-1} for the atomic composition $Al_{0.71}Fe_{0.19}Si_{0.1}$ ($Al_{7.4}Fe_2Si$) and -24.44 ± 1.4 kJ mol^{-1} for the atomic composition $Al_{0.72}Fe_{0.18}Si_{0.1}$ [21,22]. Thermal decomposition of the ternary compound α has often been observed but uncertainties remain concerning the exact nature of the decomposition reaction and the temperature at which that reaction effectively proceeds: previously proposed ranges for the decomposition temperature in literature reviews are 710–715 °C [9,13] and 855 °C [10,11]. The purpose of the present work was to obtain complete data about the crystal structure and the formation mechanism of α-AlFeSi. That is

* Corresponding author. Fax: +33 4 7244 0618.
E-mail address: jerome.roger@univ-lyon1.fr (J. Roger).

0022-4596/$ - see front matter © 2011 Elsevier Inc. All rights reserved.
doi:10.1016/j.jssc.2011.03.025

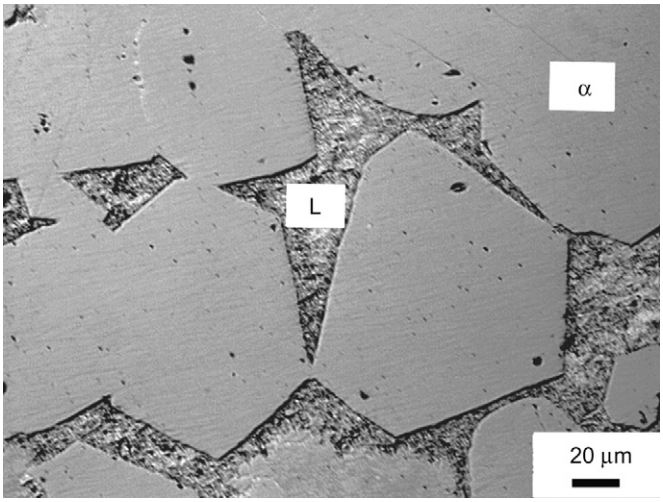

Fig. 1. Crystals of α-AlFeSi grown by precipitation from a Fe-saturated Al–Fe–Si liquid near 627 °C.

why, crystal structure examination, thermal analysis and reaction-diffusion experiments have been undertaken.

2. Experimental

Samples were prepared from pure elements: aluminium (A5LR) rod (purity > 99.8%, Strem Chemicals), iron powder (purity > 99.8%, Strem Chemicals) and monocrystalline silicon pieces (> 99.99%, Strem Chemicals). We managed to get single crystals. A sample of 6 g with initial composition Al:Fe:Si=78:10:12 mass% was prepared in three stages. In a first stage, a bar of 1.8 g with composition Fe:Al=33.3:66.7 mass% containing all the iron powder (*i.e.* 0.600 g) and 1.200 g of aluminium was cold pressed under 240 MPa. In a second stage, the silicon pieces (0.702 g) and the remaining aluminium (3.498 g) were molten together at 1073 K in an alumina crucible by direct RF coupling. In a third stage, the Al–Fe bar was dissolved into the molten Al-Si alloy. The addition to a metallic melt of alloying elements in the form of solid blocks of master alloy insures precise composition of the final alloy. This kind of procedure is commonly used by foundrymen. The liquid sample was then thermally treated as follow: 745 °C for 6 h, continuous cooling at a rate of 7° per hour up to 690 °C followed by a plateau for 40 h and quenching by dropping in cold water. This thermal treatment was applied to avoid the formation of the high temperature phase $\gamma=s_2$. Single crystals were extracted from the aluminium bare matrix that was slowly dissolved in diluted sodium hydroxide. Single-crystal intensity data were collected on an Oxford Xcalibur X-ray area-detector using Mo-$K\alpha$ radiation ($\lambda=0.71073$ Å). The programme package CrysAlisPro [23] was used to establish the angular scan conditions (φ and ω scans) for the data collections. The structure was solved by direct methods with SIR97 [24] and refined with SHELXL-97 [25]. A numerical absorption correction was made on the basis of an optimised description of the crystal faces [26]. Relevant crystal structure and refinement data are given in Table 1. The drawings were done using the programme DIAMOND [27].

For the thermal stability study, samples of different types all containing the compound α-AlFeSi as major constituent were prepared by reacting cold-pressed powder mixtures of the pure elements and equilibrating themat 727 °C for 200 h at 727 °C 200 h. For samples of type 1 (Al:Fe:Si=60:30.4:9.6 mass%) only

Table 1
Crystal data, intensity collection and refinement for $Al_{7.1}Fe_2Si$.

Collection temperature	293 K
Average chemical formula	$Al_{7.1}Fe_2Si$
Formula weight (g mol^{-1})	324.3
Crystal system	Hexagonal
Space group	$P6_3/mmc$ (no. 194)
Crystal size (mm^3)	$0.444 \times 0.322 \times 0.285$
a (Å)	12.346(2)
c (Å)	26.210(3)
V (Å^3)	3459(1)
Z	24
Calculated density (g cm^{-3})	3.736
Linear absorption coefficient (mm^{-1})	6.105
Absorption correction (analytical)	
T_{min}, T_{max}	0.217–0.330
θ range for data collection (deg.)	$3.6 \le \theta \le 29.4$
h	$-17 \le h \le 16$
k	$-16 \le k \le 16$
l	$-35 \le l \le 35$
Number of collected reflections	30,455
Number of unique reflections, R_{int}	1776, 0.065
Reflections in refinement [$I > 2\sigma(I)$]	1555
Variable parameters	125
Final R indices	
R_1, wR_2 [$I > 2\sigma(I)$]	0.029, 0.074
R_1, wR_2 (all data)	0.037, 0.079
Goodness-of-fit on F^2	1.03
($\Delta\rho$) min/max (e/Å^3)	−0.89/0.78

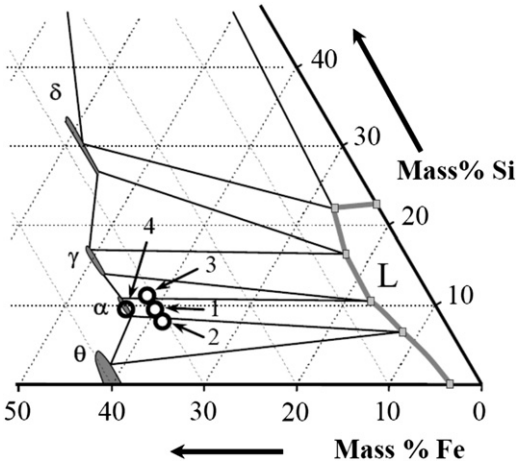

Fig. 2. Al-rich corner of the 727 °C Al–Fe–Si section, as previously established in [7].

two phases were present (α-liquid equilibrium). For samples of type 2 (Al:Fe:Si=61.7:30.4:7.9 mass%) and type 3 (Al:Fe:Si=58.3:30.4:11.3 mass%), little amounts of θ-$Al_{13}Fe_4$ (α–θ–L equilibrium) and of γ-Al_3FeSi (α–γ–L equilibrium) were also present, respectively. Samples of type 4 (Al:Fe:Si=58:32.5:9.5 mass%) were made of pure α-AlFeSi. Circles show the composition of these samples in the Al–Fe–Si section represented in Fig. 2 [16]. The samples thus prepared were either characterised by Differential Thermal Analysis (DTA) at heating/cooling rates of 5 and 2 °C min^{-1} (92-12 TGA/DTA Setaram and TGA/SDTA 851 Mettler-Toledo) or submitted to further isothermal annealing treatments. X-ray diffraction (Cu$K\alpha$ radiation), optical microscopy, scanning electron microscopy (SEM) and electron probe micro-analysis (EPMA) were used to characterize the morphology, crystal nature and composition of the phases produced (SEM and EPMA were performed at the "Centre Technologique des Microstructures—*CT*μ", Université Lyon 1).

3. Results and discussion

3.1. Crystal structure

3.1.1. Data collection and refinement

The ternary compound α-AlFeSi has been previously reported in literature to exhibit a hexagonal structure [18,28]. A crystal structure was proposed for the first time by Corby and Black [18] from anomalous-dispersion methods. Nevertheless, it was not possible for the authors to identify the silicon positions, moreover it remains some imprecisions concerning the occupation percentages and two Al isotropic factors exhibit not convenient values. As a consequence, it remains some uncertainties about this phase. That is why we undertook its structural determination. The observed reflections from the single crystal studied at room temperature could be indexed in a hexagonal unit cell, with lattice parameters $a=12.348(2)$ Å, $c=26.210(3)$ Å ($V=3459(1)$ Å^3). The Laue symmetry $P6_3/mmc$ (1 9 4) and systematic extinction conditions $000l$ ($l=2n$), and hh-$2hl$ ($l=2n$) led to the centrosymmetric space group $P6_3/mmc$, which was found to be correct during the structure determination. The structure has been solved by direct methods and least-squares refinement by using 1555 independant reflections. The five positions of iron atoms were easily identified. The other sites being occupied by silicon and aluminium atoms, the distinction of silicon atoms within these sites was more complex because of very close scattering factors. Nevertheless, we succeed in identifying the silicon atoms positions by a careful examination of both interatomic distances and coordination polyhedra. Indeed, from previous structure determinations in the system Fe–Al–Si it appears that the lowest interatomic distances between iron atoms and silicon atoms in the ternary compounds $Fe_3Al_2Si_3$, $Fe_3Al_2Si_4$ and $Fe_2Al_3Si_3$ are comprised between 2.265(1) and 2.304(3) Å [29,30]. Moreover, in the structure examinations of the ternary compounds $Fe_3Al_2Si_3$ and $Fe_3Al_2Si_4$ by Yanson et al. [29], the silicon–iron interatomic distances are equal to 2.304(3) and 2.309(3) Å. From the relevant study of the compound $Fe_2Al_3Si_3$ by Gueneau and Servant [30], it appears that the Fe–Si distances are comprised between 2.265(1) and 2.549(1) Å, while the Fe–Al distances are comprised between 2.417(1) and 2.875(1) Å. It is also important to note that the shortest Fe–Al distances in the binary compounds Fe_4Al_{13} and Fe_2Al_5 are equal to 2.374(3) and 2.34(2) Å [31,32]. As a consequence, it appears clearly that the Fe–Si bonds can be shorter than the Fe–Al bonds and that the shortest Fe–Al distances can be of about 2.32 Å: all the values below this limit should be attributed to Fe–Si bonds. In those ternary compounds, we can also notice that the Al–Si distances are comprised between 2.468(3) and 3.024(2) Å with an average value of 2.67 Å. Concerning the Al–Al bonds, the shortest distance reported is equal to 2.533(8) Å [31]. Starting from these observations the identification of silicon atoms positions was made possible. The successive steps of refinement led us to place the aluminium and silicon atoms in thirteen Al positions and in four Si positions. The distance between Si9 and Fe3 atoms is equal to 2.284(2) Å, what is unambiguously lower than the shortest Fe–Al distance (2.34(2) Å) and comprised within the Fe–Si shortest distances range (2.265(1)–2.304(3) Å). A particular situation is observed with Si19 because this atom is surrounded only by eight aluminium atoms forming a welcoming site for silicon atoms with suitable Al–Si distances comprises between 2.582(1) and 2.743(2) Å. Examination of the electronic density residuals revealed the existence of two very close positions at 0.55(3) Å from each other. According to the interatomic distances with the adjacent Fe5 atoms (2.421(2) and 2.627(16) Å) the closer position was attributed to a Si atom called Si22. Then the other site was attributed to an aluminium atom, Al21. The corresponding interatomic distances Si22–Al and Al21–Al are in good agreement with the values given earlier. In order to obtain an overall occupancy factor equal to 1 when adding the Si22 and Al21 occupancy factors, we added an occupancy constraint on these two sites. After refinement, the Si22 site occupancy factor is of about $\tau \approx 0.85(2)$, consequently the one of the Al21 site is of about $\tau \approx 0.15(2)$. Introducing isotropic displacement parameters, one silicon position, Si23, was found to be partially occupied ($\tau \approx 0.14(2)$). In the case of the Si23 atom, it appears that the distances between this atom and its Al neighbours are comprised between 2.56(3) and 2.810(2) Å, what is in good agreement with the Al–Si bonds distances previously measured in literature. Converting displacement parameters from isotropic to anisotropic, no abnormal value was observed. The displacement parameter of Si23 position was finally refined isotropically owing to the low value of its occupancy factor. Final atomic coordinates, occupancy factors and thermal displacement parameters are given in Tables 2 and 3. The main interatomic distances (Å) of α-$Al_{7.1}Fe_2Si$ and their esd's are given in Table 4.

3.1.2. Structure description

The whole representation of the crystal structure is shown in Fig. 3(a). In the partial representation of the structure presented in the Fig. 3(b), it appears that the silicon atoms are located in two different kinds of layers along the c-axis. The Si9 atoms are located in layers with z values very close to ½ and 0. The Si19, Si22 and Si23 atoms are located in the layers with $z=¼$ and $^3/_4$. We can then distinguish three kinds of alternated layers: two layers containing the silicon atoms with the Fe3 or Fe5 atoms, the third one, located between the two others, is free of silicon. Examination of the coordination polyhedral for the Fe atoms reveals that the coordination numbers (CN) of these atoms are comprised between 9 and 12 (Fig. 4). The Fe4 and Fe5 have a CN equal to 9, while Fe2 and Fe3 atoms have a CN equal to 10. Those values are generally observed for Fe–Al compounds. Fe1 has a CN equal to 12 with three distant Al14 atoms at 2.914(2) Å (Table 4). In the case of Fe_4Al_{13} and $Fe_2Al_3Si_3$ compounds, the CN of the five Fe atoms within the compounds are equal to 9, 10 and 11 [30,31]. The coordination polyhedra of Fe atoms derive of trigonal prism or antiprism with additional vertices leading to the formation of capped pentagonal faces (Fig. 4). The structure contains also four silicon atoms. Their coordination polyhedra are presented in Fig. 5. Except

Table 2
Atomic positional and isotropic displacement parameters for $Al_{7.1}Fe_2Si$.

Atom	Wyckoff site	Occ.	x	y	z	U (Å^2)
Fe1	12*k*	1	0.91923(5)	0.45961(2)	0.34064(2)	0.0088(2)[a]
Fe2	12*k*	1	0.13030(2)	0.26060(5)	0.34963(1)	0.0076(2)[a]
Fe3	12*k*	1	0.78364(3)	0.21636(3)	0.46941(2)	0.0074(2)[a]
Fe4	6*h*	1	0.20768(3)	0.41536(7)	1/4	0.0062(2)[a]
Fe5	4*f*	1	1/3	2/3	0.40024(4)	0.0071(2)[a]
Al6	24*l*	1	0.94400(8)	0.29207(7)	0.39723(3)	0.0083(2)[a]
Al7	24*l*	1	0.01168(8)	0.34367(7)	0.30190(3)	0.0074(2)[a]
Al8	12*i*	1	0	0.37215(9)	1/2	0.0088(2)[a]
Si9	12*k*	1	0.88928(5)	0.11072(5)	0.48238(4)	0.0094(2)[a]
Al10	12*k*	1	0.59596(5)	0.19193(10)	0.51695(4)	0.0066(2)[a]
Al11	12*k*	1	0.09346(10)	0.54673(5)	0.39447(4)	0.0064(2)[a]
Al12	12*k*	1	0.91595(5)	0.08405(5)	0.33197(4)	0.0080(2)[a]
Al13	12*k*	1	0.80437(11)	0.40219(5)	0.41804(4)	0.0071(2)[a]
Al14	12*k*	1	0.79742(5)	0.20258(5)	0.56847(4)	0.0075(2)[a]
Al15	12*k*	1	0.93060(5)	0.06940(5)	0.57656(4)	0.0059(2)[a]
Al16	12*k*	1	0.74851(5)	0.25149(5)	0.32564(4)	0.0085(2)[a]
Al17	12*k*	1	0.25228(5)	0.50456(11)	0.33439(4)	0.0096(2)[a]
Al18	6*h*	1	0.57051(8)	0.14103(16)	1/4	0.0109(3)[a]
Si19	6*h*	1	0.83713(7)	0.16287(7)	1/4	0.0071(3)[a]
Al20	6*h*	1	0.09091(7)	0.18182(15)	1/4	0.0088(3)[a]
Al21	6*h*	0.15(2)	0.094(3)	0.5468(16)	1/4	0.0172(9)[a]
Si22	6*h*	0.85(2)	0.1452(6)	0.5726(3)	1/4	
Si23	2*c*	0.14(2)	1/3	2/3	1/4	0.012(7)[b]

[a] U_{eq} is defined as one-third of the trace of the orthogonalized U_{ij} tensor.
[b] U_{iso}, displacement parameter of Si4 was refined isotropically.

Table 3
Anisotropic displacement parameters for $Al_{7.1}Fe_2Si$.

Atom	U_{11}	U_{22}	U_{33}	U_{23}	U_{13}	U_{12}
Fe1	0.0114(3)	0.0084(2)	0.0075(3)	−0.0015(1)	−0.0029(2)	0.0057(2)
Fe2	0.0074(2)	0.0077(3)	0.0077(3)	−0.0015(2)	−0.0007(1)	0.0038(2)
Fe3	0.0078(2)	0.0078(2)	0.0043(3)	−0.0003(1)	−0.0003(1)	0.0022(2)
Fe4	0.0076(3)	0.0086(4)	0.0028(4)	−0	−0	0.0043(2)
Fe5	0.0081(3)	0.0081(3)	0.0049(4)	−0	−0	0.0041(2)
Al6	0.0098(4)	0.0096(4)	0.0052(4)	−0.0008(3)	−0.0002(3)	0.0046(3)
Al7	0.0078(4)	0.0105(4)	0.0047(4)	−0.0006(3)	−0.0002(3)	0.0050(3)
Al8	0.0087(5)	0.0093(4)	0.0082(6)	−0.0007(2)	−0.0013(4)	0.0044(3)
Si9	0.0097(4)	0.0097(4)	0.0083(5)	−0.0008(2)	−0.0008(2)	0.0045(4)
Al10	0.0071(4)	0.0078(5)	0.0051(5)	−0.0005(4)	−0.0002(2)	0.0039(3)
Al11	0.0064(5)	0.0075(4)	0.0047(5)	−0.0005(2)	−0.0010(4)	0.0032(2)
Al12	0.0085(4)	0.0085(4)	0.0059(5)	−0.0003(2)	−0.0003(2)	0.0035(4)
Al13	0.0133(5)	0.0078(4)	0.0020(5)	−0.0004(2)	−0.0009(4)	0.0066(3)
Al14	0.0087(4)	0.0087(4)	0.0056(5)	−0.0002(2)	−0.0002(2)	0.0047(4)
Al15	0.0070(4)	0.0070(4)	0.0035(5)	−0.0005(2)	−0.0005(2)	0.0034(4)
Al16	0.0088(4)	0.0088(4)	0.0078(5)	−0.0001(2)	−0.0001(2)	0.0042(4)
Al17	0.0129(4)	0.0088(5)	0.0056(5)	−0.0007(4)	−0.0003(2)	0.0044(3)
Al18	0.0139(6)	0.0153(8)	0.0039(7)	−0	−0	0.0076(4)
Si19	0.0081(5)	0.0081(5)	0.0039(6)	−0	−0	0.0032(6)
Al20	0.0110(6)	0.0086(7)	0.0060(7)	−0	−0	0.0043(4)
Al21	0.027(3)	0.0162(9)	0.0119(9)	−0	−0	0.0135(13)
Si22	0.027(3)	0.0162(9)	0.0119(9)	−0	−0	0.0135(13)

Si9, all the Si atoms are inserted into irregular trigonal prisms with additional vertices leading to CN comprised between 8 and 12, what are common environments for this element. Indeed, the similar coordination environments for silicon atoms have been reported for $Fe_3Al_2Si_3$, $Fe_3Al_2Si_4$ and $Fe_2Al_3Si_3$ with CN comprised between 8 and 11 [29,30]. An environment with 12 members has been isolated with yttrium–rhodium–silicon compounds, for example [33,34]. Si9 atom is inserted into a pentagonal-based pyramid with one Fe3 atom at the top leading to an interatomic distance of 2.284(1) Å. In the environment of Si9, there are also 2 distant Al8 atoms at 2.843(2) Å. The corresponding CN for Si9 is equal to 8 (Fig. 5). The Si19 atom is bonded to eight Al atoms. The remarkable fact concerning this position is the absence of Si19–iron bond. The situation relative to the Al21, Si22 and Si23 is more complex. Indeed, all these positions are partially occupied. Moreover, the interatomic distances between Si22 and Si23 and between Si22 and Al21 are too short: Si22–Si23 = 2.012(7) Å, Si22–Al21 = 0.55(3) Å. When comparing the occupancy factors of Si23 and Al21, the values are found quite similar *i.e.* τ(Si23) = 0.14(2), τ(Al21) = 0.15(2). It is then clear that two situations can occur. In the first one, the Si22 site is fully occupied and the sites of Al21 and Si23 must be empty, the interatomic distances being inappropriate. In the second situation, the Si22 site is empty and the Al21 and Si23 sites are fully occupied: the occupancy factors and the interatomic bonds are in good agreement with this hypothesis (Al21–Si23 = 2.56(3) Å). As a consequence, the first arrangement with presence of Si22 atoms is obtained in 85% of the cases and the second one with the couple Al21–Si23 in 15% of the cases. The examination of the anisotropic displacement parameters of the Al17 and Al18 atoms that surround the Al21–Si22 mixed position reveals stronger variations than for the others aluminium positions (Table 3). The Fig. 6(a) and (b) shows that the Al17 and Al18 atoms have elongated displacement spheres. This is induced by the presence in their coordination polyhedra of the Al21, Si22 and Si23 atoms. Indeed, in the case of the Al17 atoms, the Al21, Si22 and Si23 positions are located on the same side of the coordination polyhedron, what induces a deformation of the anisotropic displacement along this direction. Nevertheless, this deformation is particularly oriented in the direction of Al21–Si22 (Fig. 6(a)), this can be easily understood because the distance between Al17 and Si22 is equal to 2.908(3) Å whereas the distance between Al17 and Al21 is of 3.16(3) Å. This highest value allowed Al17 atoms to move in the direction of Al21 atoms when they are presented. The same kind of situation is observed with Al18. Only one Si22–Al21 position is located in the environment of this atom (Fig. 6(b)). The distance between Al18 and Al21 is equal to 2.51(3) Å and the distance Al18–Si22 is of 3.060(7) Å. As a consequence, when the Al21 atom is absent, the Al18 atom can easily move in the direction of the Si22 atom, what explains the shape of the anisotropic displacement of this atom. We can also ask the question about the presence of silicon on the Al17 and Al18 sites. On this perspective, it appears very unlikely that silicon can be present in substitution. Considering that the distances silicon–iron are shorter than the distances iron–aluminium, the displacement ellipsoids of the atoms Al17 and Al18 should be extended toward the iron atoms, which is not the case. So, if there is a partial occupation of these sites by silicium, it could be very low. Then, the formula of this ternary phase, as deduced from structure refinement, is close to $Al_{169}Fe_{46}Si_{23}$, that is ca. $Al_{7.1}Fe_2Si$, giving a corresponding atomic ratio Al:Fe:Si of 70.9:19.3:9.8. The EPMA analysis of this phase resulting from 20 consecutive analyses on a sample synthesised at 760 °C led to the atomic ratio Al:Fe:Si = 69.8:19.0:11.2 (Table 5). Assuming that the standard deviation is comprised between 1 or 2 at%, the microanalyses are in good agreement with the composition obtained from the structural study. Nevertheless, a slightly higher content than expected is measured for silicon atoms. This deviation could be justified by the fact that the α-AlFeSi phase boundaries may change with temperature, as shown experimentally in references [16,17,20] and taken into account in the assessment of the Al–Fe–Si system by Liu and Chang [13]. It is worth noting that the content of silicon atoms decreases with temperature without modifying significantly the content of iron and that the homogeneity range is relatively narrow: from 31 to 33.3 mass% Fe (18–19.5 at% Fe) and from 8.6 to 10.9 mass% Si (10–12.5 at% Si) [16,17,20]. Then, we can deduce from these data that the crystal studied herein corresponds to the low silicon-content limit of the homogeneity range. The same kind of situation is encountered for many ternary phases in the system Fe–Al–Si [13]. This phenomenon is correlated to unit cell parameters variations [17]. In the case of α-AlFeSi, the composition variation is partially justified by the possibility to modify the occupancy factors of the Al21, Si22 and Si23 atoms. Nevertheless, this is not sufficient to explain the silicon-rich limit equal to 12.5 at% Si. The occurrence of ot her substitution sites between Si and Al atoms is likely and this is the only manner to justify the existence of such a homogeneity range.

Table 4
Main interatomic distances (Å) for $Al_{7.1}Fe_2Si$ and estimated standard deviations.

Fe1	3Al17	2.446(2)	Al7	1Al12	2.916(2)	Al15	1Fe2	2.332(2)
	3Al11	2.569(2)		1Al18	2.920(2)		2Si9	2.585(2)
	3Al10	2.645(2)		1Al16	2.922(2)		1Si9	2.622(2)
	3Al14	2.914(2)					2Al15	2.570(2)
			Al8	2Fe3	2.518(1)		1Al14	2.855(2)
Fe2	1Al15	2.332(2)		2Si9	2.843(2)		2Al12	2.918(2)
	2Al12	2.490(1)		2Al10	2.627(2)			
	2Al7	2.502(1)		2Al6	2.833(1)	Al16	1Fe4	2.405(1)
	1Al17	2.639(2)		2Al14	2.936(1)		1Si19	2.743(2)
	1Al14	2.645(2)					2Al18	2.761(2)
	1Al20	2.744(1)	Si9	1Fe3	2.284(2)		2Al6	2.896(2)
	2Al6	2.809(1)		2Si9	2.541(2)		2Al13	2.919(2)
				3Al15	2.585(2)		2Al7	2.922(2)
Fe3	1Si9	2.284(2)		2Al8	2.843(2)			
	2Al10	2.513(1)				Al17	1Fe5	2.409(1)
	2Al8	2.518(1)	Al10	1Fe3	2.513(1)		1Fe1	2.446(1)
	2Al6	2.554(1)		1Fe1	2.645(2)		1Fe2	2.639(1)
	2Al13	2.560(1)		1Al11	2.549(2)		2Al7	2.756(2)
	1Al14	2.613(2)		1Al13	2.593(2)		1Al14	2.759(2)
				2Al10	2.618(2)		1Si23	2.810(2)
Fe4	1Al11	2.337(2)		2Al8	2.627(2)		2Si22	2.908(3)
	1Al13	2.371(2)		2Al14	2.775(2)		2Al11	2.760(2)
	2Al16	2.405(1)						
	2Al7	2.453(1)	Al11	1Fe4	2.337(2)	Al18	2Fe4	2.462(1)
	1Al18	2.463(1)		1Al10	2.549(2)		1Al21	2.51(3)
	2Al6	2.684(1)		2Al6	2.737(2)		4Al16	2.761(2)
				2Al17	2.760(2)		4Al7	2.920(2)
Fe5	2Si22	2.421(2)		2Al14	2.858(1)			
	1Si23	2.687(1)				Si19	4Al7	2.582(1)
	2Al17	2.409(2)	Al12	2Fe2	2.490(1)		2Al12	2.731(2)
	1Al20	2.497(2)		1Si19	2.731(2)		2Al16	2.743(2)
	4Al7	2.519(1)		2Al20	2.851(2)			
	2Al21	2.627(16)		2Al7	2.916(2)	Al20	1Fe2	2.744(1)
				2Al15	2.918(2)		4Al12	2.851(2)
Al6	1Fe2	2.809(1)		1Al6	2.958(2)		3Al7	2.959(2)
	1Al7	2.611(2)						
	1Al11	2.737(1)	Al13	1Fe3	2.560(1)	Al21	2Fe5	2.627(16)
	1Al8	2.833(1)		2Al13	2.550(2)		1Si23	2.56(3)
	1Al14	2.914(2)		1Al10	2.593(2)		1Al18	2.51(3)
	1Al6	2.914(2)		2Al6	2.731(2)		4Al7	2.574(12)
	1Al12	2.958(2)		1Al16	2.919(2)			
						Si22	2Fe5	2.421(2)
Al7	1Fe4	2.453(1)	Al14	1Fe2	2.645(2)		4Al7	2.810(3)
	1Si19	2.582(1)		1Fe1	2.914(5)		4Al17	2.908(3)
	1Si22	2.810(3)		1Al17	2.759(2)			
	1Al21	2.574(11)		1Al10	2.775(2)	Si23	3Fe5	2.687(1)
	1Al6	2.611(2)		2Al11	2.858(1)		3Al21	2.56(3)
	1Al7	2.721(2)		2Al6	2.914(5)		6Al17	2.810(2)
	1Al17	2.756(2)		1Al8	2.936(1)			

3.2. Thermal stability

3.2.1. Thermal analysis by DTA and SDTA

Fig. 7 shows the high temperature part of DTA curves recorded for sample of types 1 to 3 with a heating rate of 5 °C min^{-1}. Whatever the phase equilibrium established at 727 °C (α–L, α–θ–L or α–γ–L), an endothermic peak was observed above this temperature. Upon first heating, the maximum of this peak appeared at 800–815 °C. On re-heating, it appeared at 780–790 °C. Upon cooling at 5 °C min^{-1}, an exothermic peak with a maximum at 700–710 °C was detected. The position of these peaks was slightly shifted when the heating/cooling rate changed from 5 to 2 °C min^{-1}. Fig. 8 shows the SDTA curves recorded on a sample of type 2 (γ–L equilibrium at 727 °C) at a heating/cooling rate of 5 °C min^{-1}. Two endothermic peaks with maxima at 615 and 800 °C were observed upon second heating; the onsets values were of 602 and 779 °C, respectively. As in DTA, the second endothermic peak was shifted towards lower temperature upon second heating (15 °C shift). Upon cooling, two exothermic peaks appeared with maxima at 710 and 580 °C; the onset values being of 724 and 593 °C, respectively. At 2 °C min^{-1}, the peaks were slightly shifted and became nearly symmetrical. The onset values were of 604 and 782 °C upon second heating and of 736 and 596 °C upon cooling. From these results, it was concluded that a reversible transformation involving the compound α-AlFeSi occurred in the temperature range 736–782 °C. Shifts in peak position with the heating/cooling rate generally characterize reactions proceeding at a slow rate. Further experiments were then conducted by isothermal diffusion in order to determine the nature and to refine the temperature of the reversible transformation. As to the 15 °C shift in peak position observed between first and subsequent re-heating by DTA or SDTA, it may be a consequence of changes in solid/solid and solid/liquid contact areas. Indeed, optical microscopy examination of a sample of type 2 after SDTA analysis revealed a larger volume fraction of liquid and a finer dispersion of crystals in the solid state.

3.2.2. Isothermal diffusion experiments

A sample of type 4 (pure α) was re-heated for 2 h at 850 °C and cooled very rapidly by oil-quenching. X-ray diffraction (XRD) characterisation revealed that α had completely disappeared and was replaced by a mixture of three solid phases θ, γ and solid Al (Fig. 8). Observation of the sample by optical microscopy confirmed the formation of a liquid phase. It thus appeared that the compound α decomposed on heating in the transformation and that three other phases θ, γ and a liquid L were involved in this transformation. Samples of type 4 were then heated for 2 h at temperatures of 770, 779, 787 and 795 °C and rapidly cooled to room temperature by oil-quenching. XRD characterisation showed that the samples heated at 770 and 779 °C only consisted of the intermetallic compound α whereas this compound was entirely converted into θ, γ (and L) in samples heated at 787 °C and above (Fig. 9). To refine further the decomposition temperature, a pure α sample was heated at 783 °C for 65 h instead of 2 h. In that experiment, partial conversion of α into γ, θ and L was identified by XRD. This gave for the compound α a decomposition temperature on heating of 781 ± 2 °C, value in excellent agreement with SDTA results at 2 °C min^{-1} (peak onset at 782 °C). The reverse reaction was finally studied. For that purpose, powder mixtures with the composition of α (type 4 samples) were reacted for 2 h at 810 °C in order to decompose α into θ, γ and L. The sample was slowly cooled down to a temperature lower than 787 °C and annealed at that temperature for 60 h. Only θ and γ were found by XRD with Al and Si in samples annealed at 778, 768 or 764 °C. Conversely, α was characterised as the major constituent in the sample annealed at 760 °C. It follows that α is effectively formed on cooling by reaction from a $\theta+\gamma+L$ mixture at temperatures equal to or lower than 762 ± 2 °C. In Table 5 are reported the analytical results obtained from EPMA (precision ± 1 wt%) on the one hand for θ, γ and L produced by decomposition of α at 787 °C and, on the other hand, for α produced by reacting a $\theta+\gamma+L$ mixture at 760 °C. It can be seen that the composition of α lies within the θ-γ-L triangle. Consequently, we can conclude that the solid compound α decomposes on heating in a ternary peritectic reaction, a four phase transformation which is invariant under constant pressure according to the phase rule and which can be written (on heating)

$$\alpha \leftrightarrow \theta+\gamma+L$$

3.2.3. Temperature of the peritectic transformation

To our knowledge, only two experimental determinations of the temperature of the above peritectic transformation were carried out in early works by Takeda and Mutuzaki in 1940 [35] and Armand in 1952 [36]. The values reported, 855 and 715 °C, respectively, were very different and a re-determination was necessary. This is why we undertook experiments specially

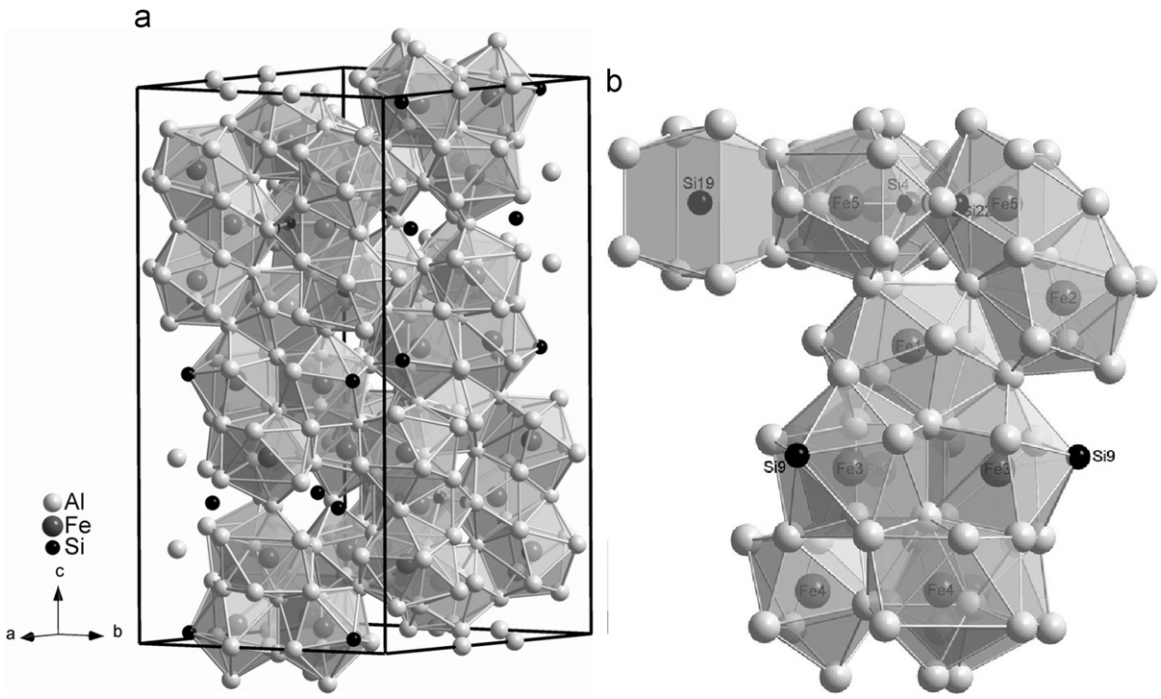

Fig. 3. Representation of the crystal structure of the α-$Al_{7.1}Fe_2Si$ compound: (a) general representation of a unit cell and (b) detailed view showing the layered disposition of polyhedra containing iron atoms in their centre.

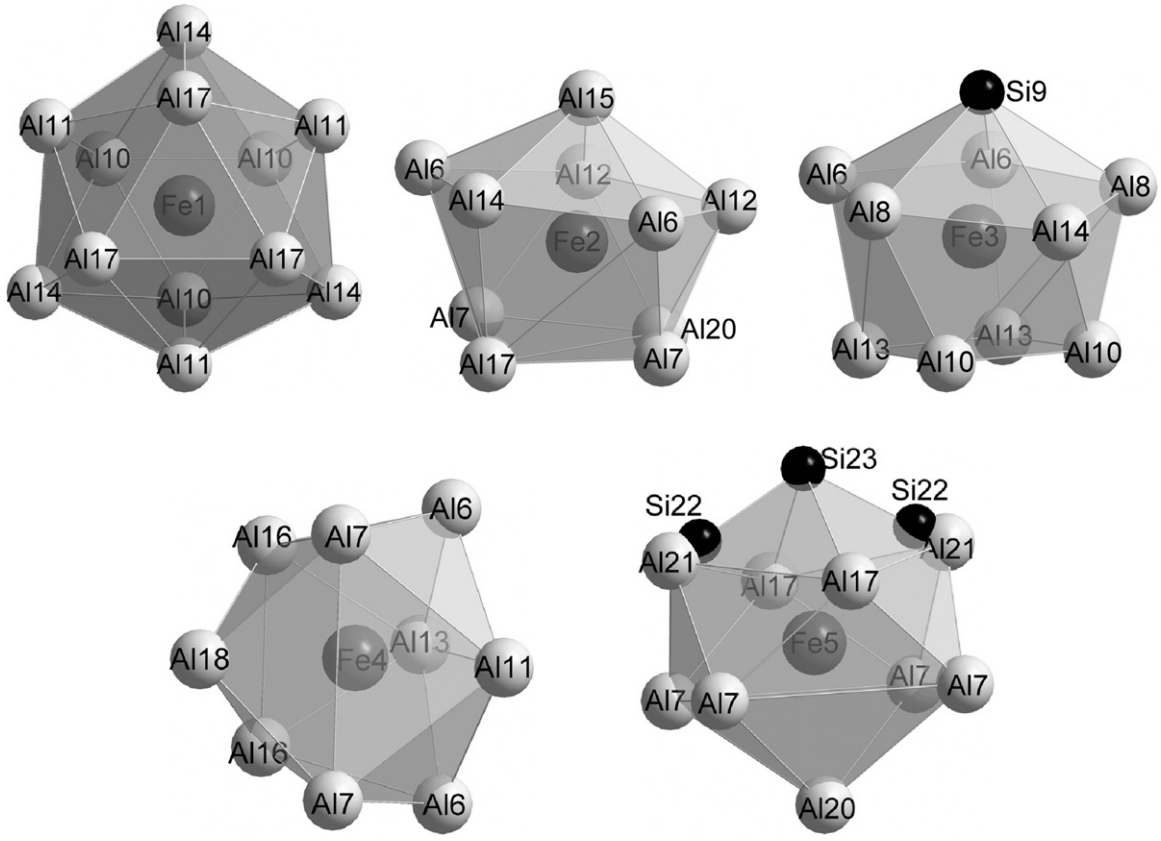

Fig. 4. Coordination polyhedra of the iron atoms.

devoted to the determination of that temperature by two complementary approaches: isothermal diffusion followed by oil quenching and thermal analysis at different heating/cooling rates. Both static and dynamic approaches gave self-consistent results. Decomposition of α has been observed at 783 °C and above. The reverse reaction has been observed at 760 °C and below. The transformation is then reversible and its temperature under atmospheric pressure is of 772 ± 12 °C. Krendelsberger et al. [7]

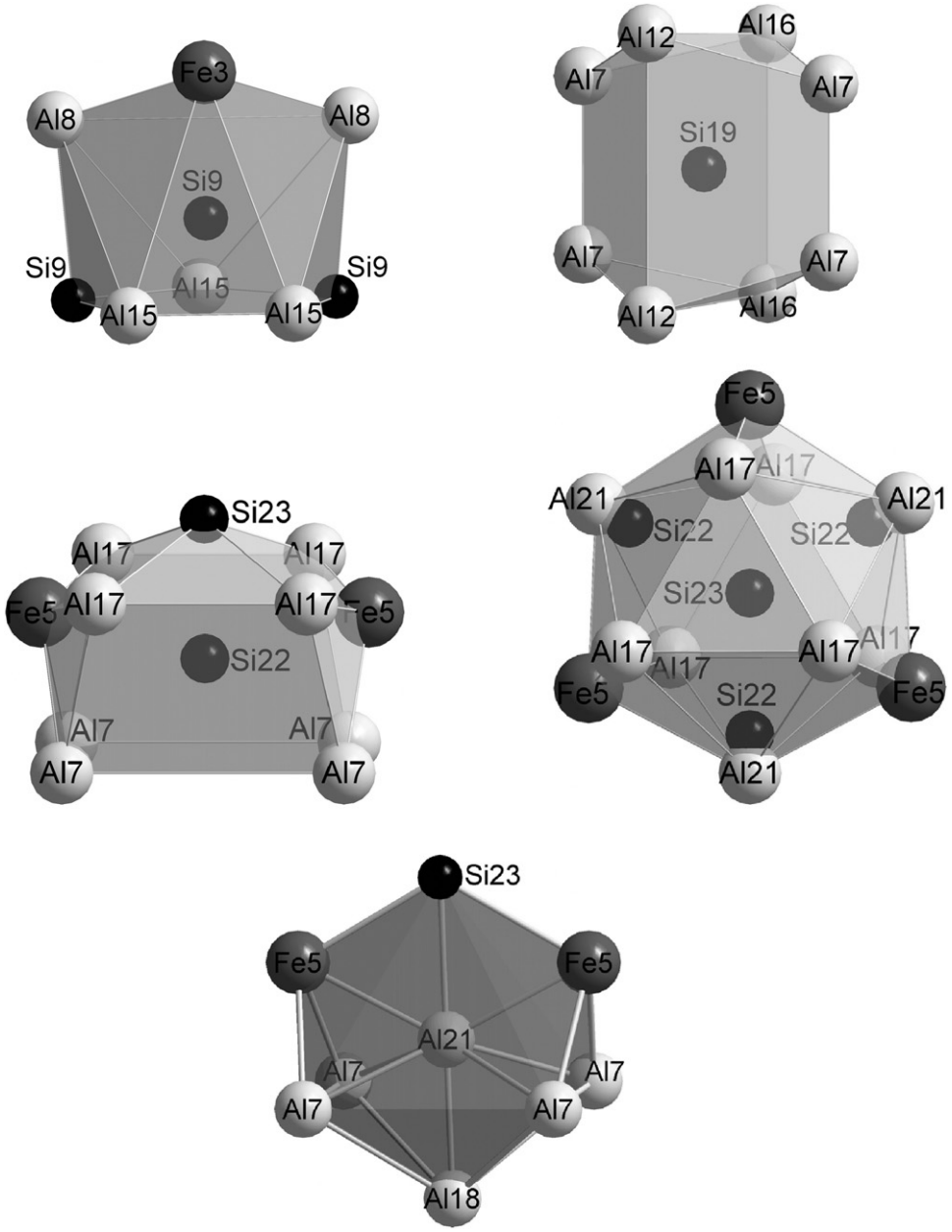

Fig. 5. Coordination polyhedra of the silicon and Al21 atoms.

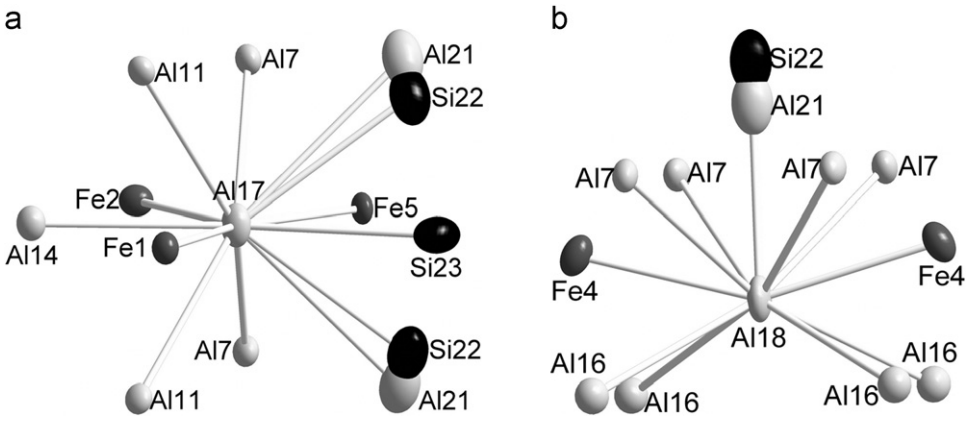

Fig. 6. Coordination polyhedra and thermal ellipsoid: (a) Al17 and (b) Al18 atoms.

Table 5
Composition of the four phases involved in the invariant transformation studied.

Phases	Al wt% (at%)	Fe wt% (at%)	Si wt% (at%)
θ (787 °C)	58.6 ± 1 (73.1 ± 1.5)	38.0 ± 1 (22.9 ± 0.7)	3.4 ± 1 (4.0 ± 1.0)
γ (787 °C)	52.7 ± 1 (64.6 ± 1.3)	34.6 ± 1 (20.5 ± 1.7)	12.7 ± 1 (14.9 ± 1.2)
L (787 °C)	75.9 ± 1 (81.6 ± 1.1)	12.6 ± 1 (6.5 ± 0.5)	11.5 ± 1 (11.9 ± 1.0)
α (760 °C)	57.8 ± 1 (69.8 ± 1.2)	32.6 ± 1 (19.0 ± 0.6)	9.6 ± 1 (11.2 ± 0.9)

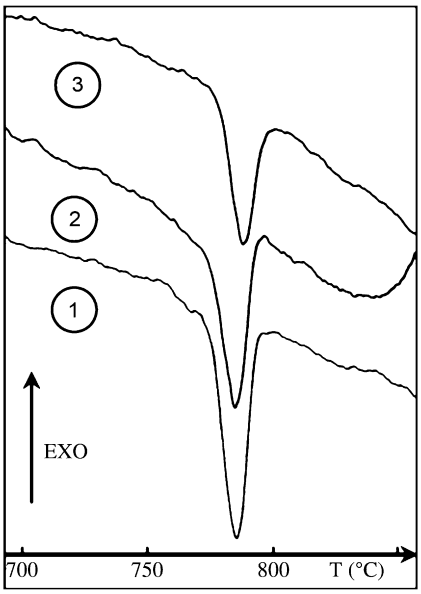

Fig. 7. DTA curves (high temperature part) recorded at a heating rate of 5 °C min^{-1} for sample of types 1–3 (α–L, α–θ–L and α–γ–L at 727 °C).

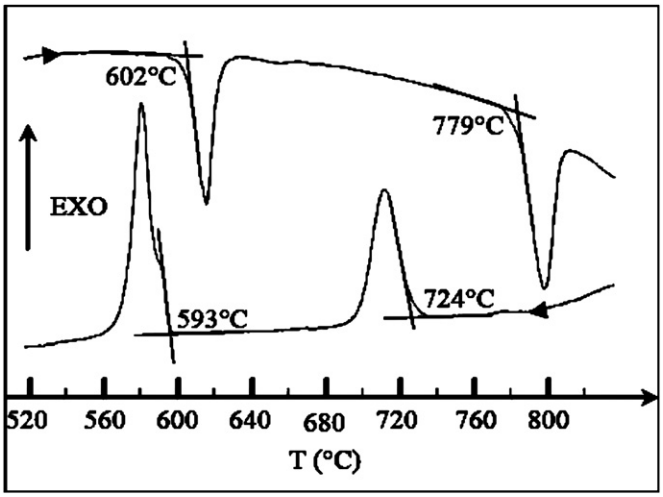

Fig. 8. SDTA curves recorded on a sample of type 2 (γ–L equilibrium at 727 °C) at a heating/cooling rate of 5 °C min^{-1}.

who were the first to know this result (through private communication) corroborated it.

4. Conclusion

The structural and thermochemical properties of the ternary compound α-AlFeSi were carefully investigated. The crystal chemistry of this phase was precisely examined on single crystal leading to the average chemical formula $Al_{7.1}Fe_2Si$. For the first time, it was possible to identify the crystallographic positions of silicon atoms. α-AlFeSi exhibits a hexagonal symmetry with unit cell parameters equal to $a=12.345(2)$ Å and $c=26.210(3)$ Å. The main part of the structure is fully ordered. Nevertheless, among the four silicon positions, two positions are close and partially occupied with a reciprocal dependency of the occupancy factors. For one of them, a neighbouring aluminium position is added when the silicon atom is absent. The homogeneity range previously identified for this phase can be partially explained by this substitution mechanism. Nevertheless, it is not sufficient to justify the Si-rich limit of the α-AlFeSi homogeneity range that reaches up to 12.5 at% at 727 °C and the existence of others substitution sites between aluminium and silicon atoms should be considered.

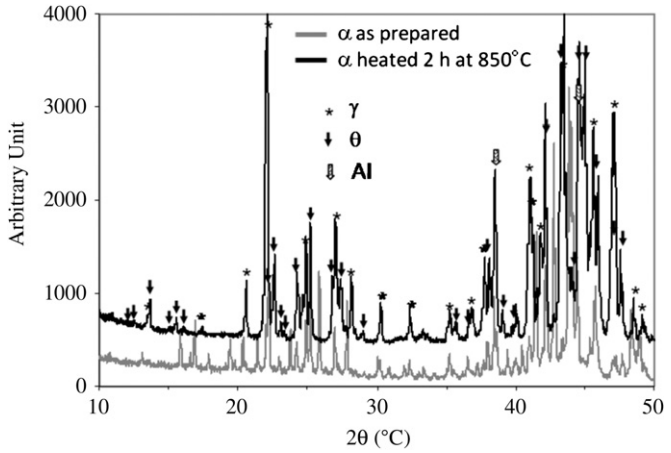

Fig. 9. XRD spectra for: (a) pure α as synthesised at 727 °C; (b) Al, θ and γ decomposition products after 2 h re-heating at 850 °C.

Combining the results from both Differential Thermal Analysis and isothermal reaction-diffusion experiments has led to the conclusion that the ternary compound α-AlFeSi decomposes on heating according to the ternary peritectic transformation:

$$\alpha \leftrightarrow \theta + \gamma + L$$

Under atmospheric pressure (101 350 Pa), the temperature of this reversible transformation is of 772 ± 12 °C.

Supporting information available

Further details on the crystal structure investigations may be obtained from the Fachinformationszentrum Karlsruhe, 76344 Eggenstein-Leopoldshafen, Germany (fax: (49) 7247 808 666; e-mail: crysdata@fiz.karlsruhe.de), on quoting the depository number CSD-422224.

Acknowledgments

The authors wish to thank E. Janneau (Centre de diffraction Henri Longchambon, Université Lyon1) for his assistance in X-ray intensity data collection.

References

[1] L.M. Kubalova, I.A. Sviridov, O.Y. Vasilyeva, V.I. Fadeeva, J. Alloys Compd. 434 (2007) 467–471.
[2] O.A. Lambri, J.I. Pérez-Landazabal, G.J. Cuello, J.A. Cano, V. Recarte, C. Siemers, I.S. Golovin, J. Alloys Compd. 468 (2009) 96–102.
[3] P. Novak, A. Michalcova, M. Voderova, M. Sima, J. Serak, D. Vojtech, K. Wienerova, J. Alloys Compd. 493 (2010) 81–86.

[4] P. Novak, V. Knotek, M. Voderova, J. Kubasek, J. Serak, A. Michalcova, D. Vojetch, J. Alloys Compd. 497 (2010) 90–94.
[5] V. Stefaniay, A. Griger, T. Turmezey, J. Mater. Sci. 22 (1987) 539–546.
[6] T. Maitra, S.P. Gupta, Mater. Charact. 49 (2003) 293–311.
[7] N. Krendelsberger, F. Weitzer, J.C. Schuster, Metall. Mater. Trans. A 38 (2007) 1681–1691.
[8] A. Lendvai, Thermochim. Acta 93 (1985) 681–684.
[9] L.F. Mondolfo, Aluminium and Alloys, Structure and Properties, Butterworth, London, 1976.
[10] V.G. Rivlin, G.V. Raynor, Int. Met. Rev. 3 (1981) 133–152.
[11] G. Ghosh, in: G. Petzow, G. Effenberg (Eds.), Ternary Alloys, vol. 5, VCH, Weinheim, , 1988.
[12] V. Raghavan, J. Phase Equilibria Diffusion 30 (2009) 184–188.
[13] Z.K. Liu, Y.A. Chang, Metall. Mater. Trans. A 30A (1999) 1081–1095.
[14] Y. Du, J.C. Schuster, Z.K. Liu, R. Hu, P. Nash, W. Sun, W. Zhang, J. Wang, L. Zhang, C. Tang, Z. Zhu, S. Liu, Y. Ouyang, W. Zhang, N. Krendelsberger, Intermetallics 16 (2008) 554–570.
[15] D.V. Malakhov, D. Panahi, M. Gallerneault, CALPHAD: Comput. Coupling Phase Diagrams Thermochem. 34 (2) (2010) 159–166.
[16] S. Pontevichi, F. Bosselet, F. Barbeau, M. Peronnet, J.C. Viala, J. Phase Equilib. 25 (2004) 528–537.
[17] T. Turmezey, V. Stefaniay, A. Griger, Key Eng. Mater. 44–45 (1990) 57–68.
[18] R.N. Corby, P.J. Black, Acta Crystallogr. B33 (1977) 3468–3475.
[19] P. Liu, Key Eng. Mater. 44 (1990) 69–86.
[20] A. Griger, Powder Diffr. 2 (1987) 31–35.
[21] M. Vybornov, P. Rogl, F. Sommer, J. Alloys Compd. 247 (1997) 154–157.
[22] Y. Li, P. Ochin, A. Quivy, P. Telolahy, B. Legendre, J. Alloys Compd. 298 (2000) 198–202.
[23] CrysAlisPro, Oxford Diffraction Ltd.,Version 1.171.33.66, Analytical numeric absorption correction using a multifaceted crystal model based on expressions derived by R.C. Clark, J.S. Reid. (Acta Cryst. A51 (1995) 887–897).
[24] A. Altomare, M.C. Burla, M. Camalli, B. Carrozzini, G.L. Cascarano, C. Giacovazzo, A. Guagliardi, A.G.G. Moliterni, G. Polidori, R. Rizzi, J. Appl. Crystallogr. 32 (1999) 115–119.
[25] G.M. Sheldrick, SHELXL-97: Program for the Refinement of Crystal Structure, University of Göttingen, Göttingen, 1997.
[26] R.C. Clark, J.S. Reid, Acta Crystallogr. A51 (1995) 887–897.
[27] K. Brandenburg, DIAMOND, Version 3.2, , 2010.
[28] K. Robinson, P.J. Black, Philos. Mag. 44 (1953) 1392–1397.
[29] T.I. Yanson, M.B. Manyako, O.I. Bodak, N.V. German, O.S. Zarechnyuk, R. Cerny, J.V. Pacheco, K. Yvon, Acta Crystallogr. C52 (1996) 2964–2967.
[30] C. Gueneau, C. Servant, Acta Cryst. C51 (1995) 2461–2464.
[31] J. Grin, U. Burkhardt, M. Ellner, Z. Kristallogr. 209 (1994) 479–487.
[32] U. Burkhardt, Y. Grin, M. Ellner, Acta Crystallogr. B50 (1994) 313–316.
[33] L. Piccard, D. Piccard, J. Less Common Met. 109 (1985) 229–232.
[34] J.M. Moreau, D. Piccard, L. Piccard, Acta Cryst. C40 (1984) 1311–1312.
[35] H.P. Takeda, K. Mutuzaki, Tetsu To Hagane 26 (1940) 335–361.
[36] M. Armand, C.R. Acad. Sci. Paris 235 (1952) 1506–1508.